Available online at www.sciencedirect.com
ScienceDirect
Journal of Computational Physics 220 (2006) 41–58
JOURNAL OF COMPUTATIONAL PHYSICS
www.elsevier.com/locate/jcp

Idempotent filtering in spectral and spectral element methods

Alex Kanevsky [a,*], Mark H. Carpenter [b], Jan S. Hesthaven [a]

[a] Division of Applied Mathematics, Brown University, Box F, Providence, RI 02912, USA
[b] Aeronautics and Aeroacoustic Methods Branch, NASA Langley Research Center, Hampton, VA 23681-0001, USA

Received 11 April 2005; received in revised form 5 January 2006; accepted 5 May 2006
Available online 10 July 2006

Abstract

The comparison of numerical results for implicit–explicit and fully explicit Runge–Kutta time integration methods for a nozzle flow problem shows that filtering can significantly degrade the accuracy of the numerical solution for long-time integration problems. We demonstrate analytically and numerically that filtering-in-time errors become additive for $\|u_N(x,t+k\Delta t)-u_N(x,t)\| \ll \|u_N(x,t)\|$ when nonidempotent filters are used, and suggest the development and implementation of idempotent filters.

Keywords: Idempotent; Modal filters; Spectral methods; Implicit-explicit (IMEX) Runge-Kutta

1. Introduction

In the last decade, significant attention has been paid to modal filtering in spectral methods [2,4,8,9]. Filtering is popular in spectral and spectral element-type methods for several reasons. Firstly and most importantly, it stabilizes the numerical approximation and results in a more robust method. Furthermore, for discontinuous functions, filtering can recover high-order accuracy at the points of discontinuity [11,10] and in the smooth regions away from the discontinuity [23]. In the early 1990s, Gottlieb et al. [11] showed that the Gibbs phenomenon, which is associated with the reconstruction of discontinuous functions, could be overcome by accelerating the rate of convergence of the reconstruction using Gegenbauer polynomials. Since then, a lot of work has followed along similar lines. A recent review of filtering in spectral methods can be found in [8,13].

However, there are still many unresolved issues related to filtering, e.g., it is not clear how to choose a filter for the problem at hand. What filter order should one use? Should the filter be applied once or more per time step or perhaps once every several time steps? What is the effect of applying a filter repeatedly on the accuracy of the approximation?

* Corresponding author. Tel.: +1 781 956 3422.
E-mail addresses: kanevsky@dam.brown.edu, kanevsky@cims.nyu.edu (A. Kanevsky), Mark.H.Carpenter@nasa.gov (M.H. Carpenter), Jan.Hesthaven@Brown.edu (J.S. Hesthaven).

0021-9991/$ - see front matter
doi:10.1016/j.jcp.2006.05.014

We aim to address some of these issues in this paper, and give some guidelines concerning how filters should be designed and applied in practice for spectral and spectral element methods. We will restrict the theory and numerical examples to two types of low-pass filters [21]: the sharp-cutoff or step-function filter used in classical dealising methods [4] and the exponential filter. However, the ideas and analysis presented may be applied to a more general class of filters.

One of the outcomes of comparing numerical test results using explicit Runge–Kutta (ERK) time-integration methods [5] to those using implicit–explicit (IMEX-RK) methods [18] is the realization that filtering may severely degrade the accuracy of the approximation when applied for a large number of time steps. We can see in Fig. 1.1 that the IMEX-RK tests, which were run at time steps an order of magnitude larger (on average) than the ERK tests ($\Delta t_{\mathrm{ERK}} \approx 8.56 \times 10^{-4}$, $\Delta t_{\mathrm{IMEX-RK}} \approx 6.69 \times 10^{-3}$), show superior accuracy, especially in the case of relatively low-order exponential filters [16,17]. We integrated to a finite physical time $T = 40$ for both the IMEX-RK and the ERK tests. The details of the physical and numerical setup for the nozzle flow test case appear in Appendix A.

In Section 2, we review the underlying theory behind filtering in spectral methods. In Section 3, we analyze the net effect of filtering on the accuracy of the numerical approximation, and show that filtering a numerical approximation with the property $\|u_N(x, t + k\Delta t) - u_N(x, t)\| \ll \|u_N(x, t)\|$ results in a multiplicative filtering process, which is supported by numerical tests in Section 4. This observation leads us to suggest that time-dependent filters be developed to control filtering-in-time errors. We propose time-dependent exponential filters in Section 5, and construct filters whose filter order, $p(t)$, is a function of time. We then show that if $p(t)$ can be properly controlled, we can overcome the potentially multiplicative net effect of filtering in time. The control

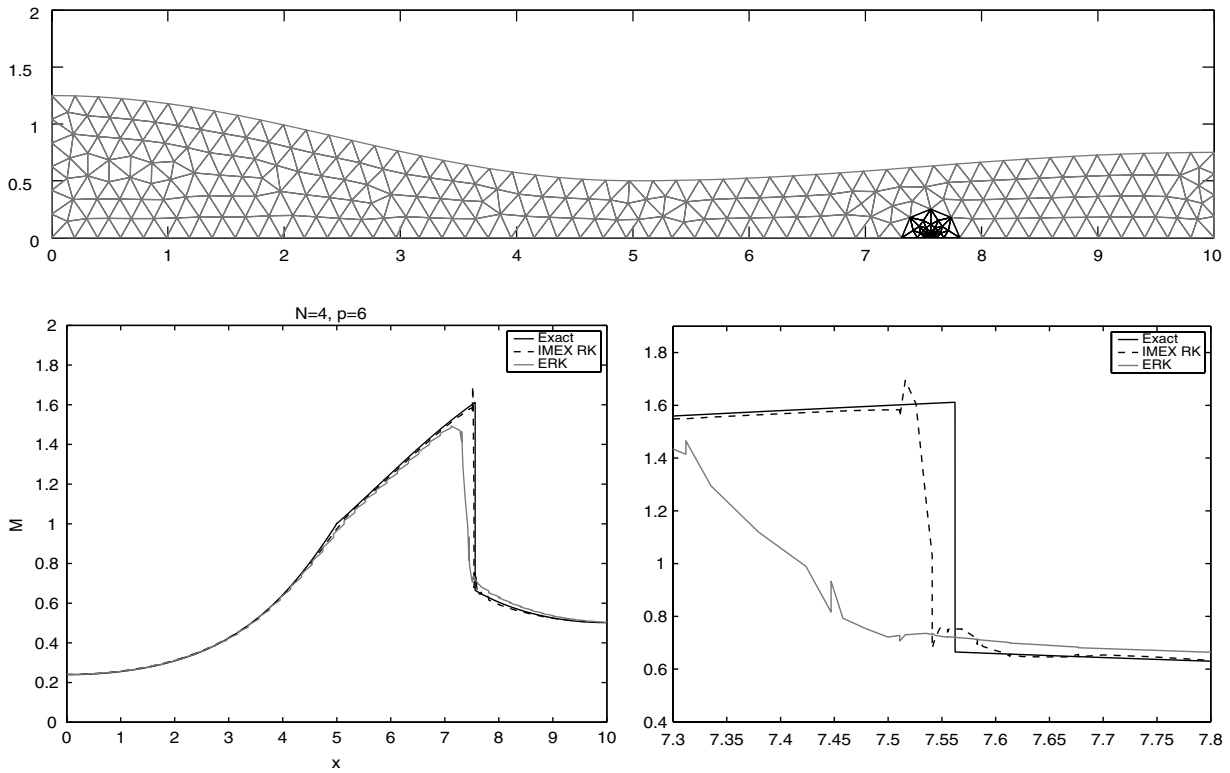

Fig. 1.1. The top image is the mesh used for the two-dimensional steady-state converging-diverging nozzle flow tests. The black region is solved implicitly when using the IMEX-RK scheme, and explicitly when using the ERK scheme. The exact steady-state solution to the Euler equations has a shock at $x \cong 7.56$. The two figures below compare the Mach number profiles at the centerline of the nozzle, $y = 0$, for the ERK, IMEX-RK, and analytic solutions. The bottom-right figure is a close-up of the shock region in the bottom-left figure. The polynomial degree $N = 4$ on each element and the order of the exponential filter $p = 6$.

strategy for $p(t)$ is based on the worst-case scenario, purely multiplicative filtering. Finally, we discuss the results and make concluding remarks in Section 6.

2. Filtering

Our goal is to approximate the exact solution $u(x,t)$ of a conservation law in the form

$$\frac{\partial u(x,t)}{\partial t}+\frac{\partial f(u(x,t))}{\partial x}=0. \tag{2.1}$$

We express $u(x,t)$ as an infinite series of basis functions $\phi_n(x)$

$$u(x,t)=\sum_{n=0}^{\infty}\hat{u}_n(t)\phi_n(x). \tag{2.2}$$

In spectral methods, we project $u(x,t)$ to the finite-dimensional space $P_N\in\{\phi_n(x)\}_{n=0}^{N}$ and get the truncated approximate solution

$$u_N(x,t)=\mathscr{P}_{\mathscr{N}}u(x,t)=\sum_{n=0}^{N}\hat{u}_n(t)\phi_n(x). \tag{2.3}$$

$\mathscr{P}_{\mathscr{N}}u(x,t)\in P_N$, where P_N is spanned by the smooth basis functions $\phi_n(x)$, which form an L^2-complete basis.

When using spectral methods to solve nonlinear conservation laws, nonsmooth solutions may develop. Even if nonsmooth solutions do not develop, smooth solutions with sharp gradients may develop, as in the case of high-Reynolds number fluid flows. If there is not enough spatial resolution in the numerical approximation to adequately resolve such solutions (which will always be the case in the presence of shock/s), the Gibbs phenomenon will develop. Not only will the Gibbs oscillations reduce the spectrally convergent rate of decay of the global expansion coefficients (exponential rate) to a linear rate of decay (N^{-1}), but the nonlinear interaction of the Gibbs oscillations with the numerical solution will increase the energy of all the modes, thereby resulting in nonlinear instability (unbounded growth of high-frequency energy in time). Thus, the numerical method may lose its beautiful convergence properties and become unstable.

We can add a term to our original PDE (2.1) that dissipates the high-frequency energy components and therefore controls the instability

$$\frac{\partial u(x,t)}{\partial t}+\frac{\partial f(u(x,t))}{\partial x}=\epsilon(-1)^{p+1}\frac{\partial^{2p}u}{\partial x^{2p}}. \tag{2.4}$$

Although adding artificial dissipation to (2.1) will stabilize the method, it is costly and may introduce restrictions on the stable time step.

Instead, we follow the approach originally introduced in [19,20] and add dissipation by applying a modal filter to the numerical approximation at regular intervals. The filtered approximation is

$$\mathscr{F}_{\mathscr{N}}u_N(x,t)=\sum_{n=0}^{N}\sigma\left(\frac{n}{N}\right)\hat{u}_n(t)\phi_n(x), \tag{2.5}$$

where $\sigma(\eta)$ is the filter kernel.

Let us introduce two commonly used filter functions, which we will refer to in subsequent sections:

1. *Exponential filter*

$$\sigma\left(\frac{n}{N}\right)=\begin{cases}1, & 0\leqslant n\leqslant N_c,\\ \exp\left[-\alpha\left(\frac{n-N_c}{N-N_c}\right)^p\right], & N_c<n\leqslant N,\end{cases} \tag{2.6}$$

where p is the order of the filter, $\alpha=-\log\epsilon$ (ϵ is the machine zero), and N_c is the cutoff mode.

2. *Sharp-cutoff* or *step-function filter*

$$\sigma\left(\frac{n}{N}\right) = \begin{cases} 1, & 0 \leqslant n \leqslant N_c, \\ 0, & N_c < n \leqslant N, \end{cases} \tag{2.7}$$

where N_c is the cutoff mode.

3. From multi-modes to uni-mode

Let us assume that $\|u_N(x,t+\Delta t) - u_N(x,t)\| \ll \|u_N(x,t)\| \Rightarrow u_N(x,t+\Delta t) \approx u_N(x,t)$. For now, we restrict the time step, Δt, to be constant, and assume that the filter kernel, $\sigma(\eta)$, does not change with time.

After applying the filter once at the end of the time step, the filtered approximation becomes:

$$\tilde{u}_N(x,t+\Delta t) = \mathscr{F}_{\mathscr{N}} u_N(x,t+\Delta t) \cong \mathscr{F}_{\mathscr{N}} u_N(x,t) \tag{3.8}$$

$$= \sum_{n=0}^{N} \sigma\left(\frac{n}{N}\right) \hat{u}_n(t)\phi_n(x). \tag{3.9}$$

If we filter once again at the end of the next time step, we have

$$\tilde{u}_N(x,t+2\Delta t) = \mathscr{F}_{\mathscr{N}} u_N(x,t+2\Delta t) \cong \mathscr{F}_{\mathscr{N}} \tilde{u}_N(x,t+\Delta t) \tag{3.10}$$

$$\cong \mathscr{F}_{\mathscr{N}}(\mathscr{F}_{\mathscr{N}} u_N(x,t)) = \sum_{n=0}^{N} \sigma\left(\frac{n}{N}\right)\left(\sigma\left(\frac{n}{N}\right)\hat{u}_n(t)\phi_n(x)\right) \tag{3.11}$$

$$= \sum_{n=0}^{N} \sigma^2\left(\frac{n}{N}\right)\hat{u}_n(t)\phi_n(x) \tag{3.12}$$

$$= \mathscr{F}^2_{\mathscr{N}} u_N(x,t). \tag{3.13}$$

Repeating this process k times, and assuming that $\|u_N(x,t+k\ \Delta t) - u_N(x,t)\| \ll \|u_N(x,t)\|$ we have

$$\tilde{u}_N(x,t+k\Delta t) \cong \mathscr{F}^k_{\mathscr{N}} u_N(x,t) = \sum_{n=0}^{N} \sigma^k\left(\frac{n}{N}\right)\hat{u}_n(t)\phi_n(x) \tag{3.14}$$

$$= \sum_{n=0}^{N} \tilde{\sigma}_{k\Delta t}\left(\frac{n}{N}\right)\hat{u}_n(t)\phi_n(x). \tag{3.15}$$

The net effect of filtering k times is represented by the *net filter* $\tilde{\sigma}_{k\Delta t}(\eta)$, which we define as

$$\tilde{\sigma}_{k\Delta t}(\eta) = \sigma^k(\eta). \tag{3.16}$$

We now assume that our filter kernel is an exponential filter with $N_c = 0$

$$\sigma(\eta) = \exp(-\alpha\eta^p). \tag{3.17}$$

Therefore,

$$\tilde{u}_N(x,t+k\Delta t) \cong \mathscr{F}^k_{\mathscr{N}} u_N(x,t) = \sum_{n=0}^{N} \sigma^k\left(\frac{n}{N}\right)\hat{u}_n(t)\phi_n(x) \tag{3.18}$$

$$= \sum_{n=0}^{N} \exp\left(-\alpha k\left(\frac{n}{N}\right)^p\right)\hat{u}_n(t)\phi_n(x) \tag{3.19}$$

i.e. the net filter becomes

$$\tilde{\sigma}_{k\Delta t}(\eta) = \sigma^k(\eta) = \exp(-\alpha k\eta^p). \tag{3.20}$$

Filtering repeatedly results in an multiplicative process, under the assumptions stated at the beginning of this section. In fact, a purely multiplicative filtering process, which is represented by the net filter, is the upper-bound on filtering time-dependent problems, resulting in a net filter kernel that grows in strength (area

under the net filter kernel vs. mode number curve diminishes) with each time step, and is equal to σ^k after k steps. We can clearly see from this analysis that as the number of time steps k grows large, which we expect in long-time simulations, the net filter kernel can have an extremely strong, crippling effect on the accuracy of the numerical solution.

For spectral element methods, it is common to use polynomial approximations of degree $N = 4$ to $N = 16$ on each subdomain. Filtering regularly can effectively zero out many of the modes, thereby potentially reducing polynomial approximations of degree $N = 4$ to $N = 16$ to much lower-degree polynomials. The same holds for classical spectral methods with polynomial degree $N = 128, 256, \ldots$, although it is more difficult to "see" the loss in accuracy. We demonstrate the effects of using nonidempotent filters in Section 4, where we conduct a number of numerical experiments.

4. Numerical experiments

In order to validate the analysis in Section 3, we perform the following set of numerical experiments. First, we repeat the nozzle flow test case using small time steps, $\Delta t = 1 \times 10^{-6}$, and polynomials of degree $N = 4$ on each element. We use an initial condition which is very far from the exact steady-state solution (the IC is a linear profile connecting the inflow and outflow BCs), and are therefore solving a time-dependent problem. Since the time steps are very small, the solution will change very slowly with respect to the time step number, k, and should adhere to the above theory. We apply a nonidempotent exponential filter (3.17) and plot the results after $k = 10^4$ time steps.

Fig. 4.3(a) and (b) shows that the nonidempotent exponential filter degrades the accuracy of the numerical solution, just as we predicted above. In fact, we see a staircase phenomenon develop. The approximations, which originally start out as polynomials of degree $N = 4$, are filtered into 0th-degree polynomials on each subdomain (piecewise-constants) by the nonidempotent filter of order $p = 6$, resulting in a solution that looks flat on each element (Fig. 4.3). The staircase-looking results from this numerical experiment support Fig. 3.2, which shows plots of the net filter versus mode number for the nonidempotent exponential filter based on (3.20) for varying number of time steps. Fig. 3.2(e), corresponding to $k = 10^4$ time steps, shows that the filters of order $p = 6$ and $p = 8$ zero out virtually all but the first mode for polynomials of degree four. Even the $p = 16$ nonidempotent exponential filter zeros out all but the first 2 modes after 10^4 steps.

Table 4.1 supports the assumption that $\|u_N(x, t + k\Delta t) - u_N(x, t)\| \ll \|u_N(x, t)\|$ for the Mach number for the nozzle flow example described above. The second column shows results for the average value of $\frac{\|M(x,t+\Delta t)-M(x,t)\|_2}{\|M(x,t)\|_2}$ for different values of k, while the fifth column shows results for $\frac{\|M(x,t+k\Delta t)-M(x,t)\|_2}{\|M(x,t)\|_2}$. Note that $\frac{\|M(x,t+k\Delta t)-M(x,t)\|_2}{\|M(x,t)\|_2} \ll 1$ for all values of k up to 10^4.

Additional evidence of the staircase phenomenon can be seen in the ERK Mach number profile in Fig. 1.1. The onset of staircasing is evident in the ERK approximation (gray) which was integrated for 46,741 time steps. The IMEX-RK approximation (dashed) was integrated for 5975 time steps and does not exhibit staircasing at this scale, although it does exhibit staircasing at higher magnifications.

We perform the same exact numerical experiment we carried out for the nonidempotent exponential filter to test the idempotent sharp-cutoff filter defined in Section 2 (2.7). We use $N_c = N - 1$, polynomial degree $N = 4$ and $\Delta t = 1 \times 10^{-6}$. We can see from the results in Fig. 4.3(c) and (d) that the sharp-cutoff filter is indeed idempotent and does not result in staircasing, since it only cuts off the highest mode $n = N$. However, if the solution is smooth and well resolved, filtering is not needed.

We repeat the filtering experiments conducted above for one more test case. Fig. 4.4 compares the nonidempotent exponential filter of order $p = 6$ to the sharp-cutoff filter with $N_c = N - 1$ for the two-dimensional cylinder flow test case at $Re = 125$ (refer to Appendix A). The simulation is restarted at time $t = 150$, at which point the flow is fully-developed with periodic vortex shedding occurring. We apply both types of filters for 10^4 time steps, and compare the resulting Mach contours (filtered at every stage). We

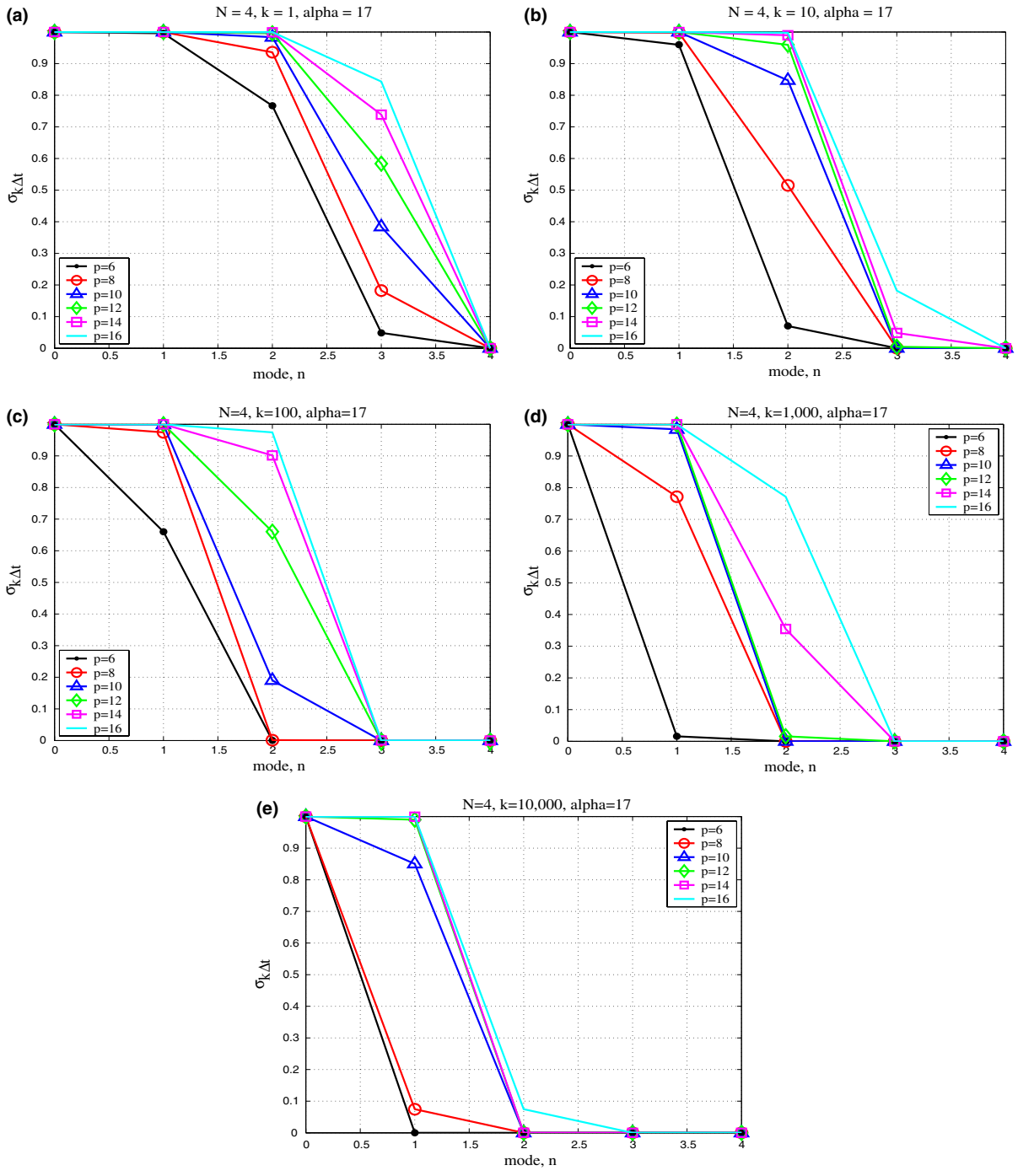

Fig. 3.2. Net filter strength versus mode number for nonidempotent exponential filter (3.20) of order $p = 6, 8, 10, 12, 14, 16$. Number of time steps $k = 1$ (top-left), $k = 10$ (top-right), $k = 10^2$ (middle-left), $k = 10^3$ (middle-right), and $k = 10^4$ (bottom). Polynomial degree $N = 4$, $\alpha = 17$.

can clearly see staircasing when the nonidempotent exponential filter is used (Fig. 4.4(a)), and no staircasing when the sharp-cutoff filter is used (Fig. 4.4(b)). The time steps, $\Delta t = 1 \times 10^{-6}$, and polynomials degree is $N = 4$.

Table 4.1
Measures of $\|u_N(x,t+k\Delta t)-u_N(x,t)\|_2$ and $\|u_N(x,t)\|_2$ for Mach number (nozzle flow test)

k	Avg. $\frac{\|M(x,t+\Delta t)-M(x,t)\|_2}{\|M(x,t)\|_2}$	$\|M(x,t+k\Delta t)-M(x,t)\|_2$	$\|M(x,t)\|_2$	$\frac{\|M(x,t+k\Delta t)-M(x,t)\|_2}{\|M(x,t)\|_2}$
10^1	1.53E−05	5.69E−05	3.73E−01	1.53E−04
10^2	1.27E−05	4.74E−04	3.73E−01	1.27E−03
10^3	3.66E−06	1.36E−03	3.73E−01	3.65E−03
10^4	4.60E−07	1.44E−03	3.73E−01	3.85E−03

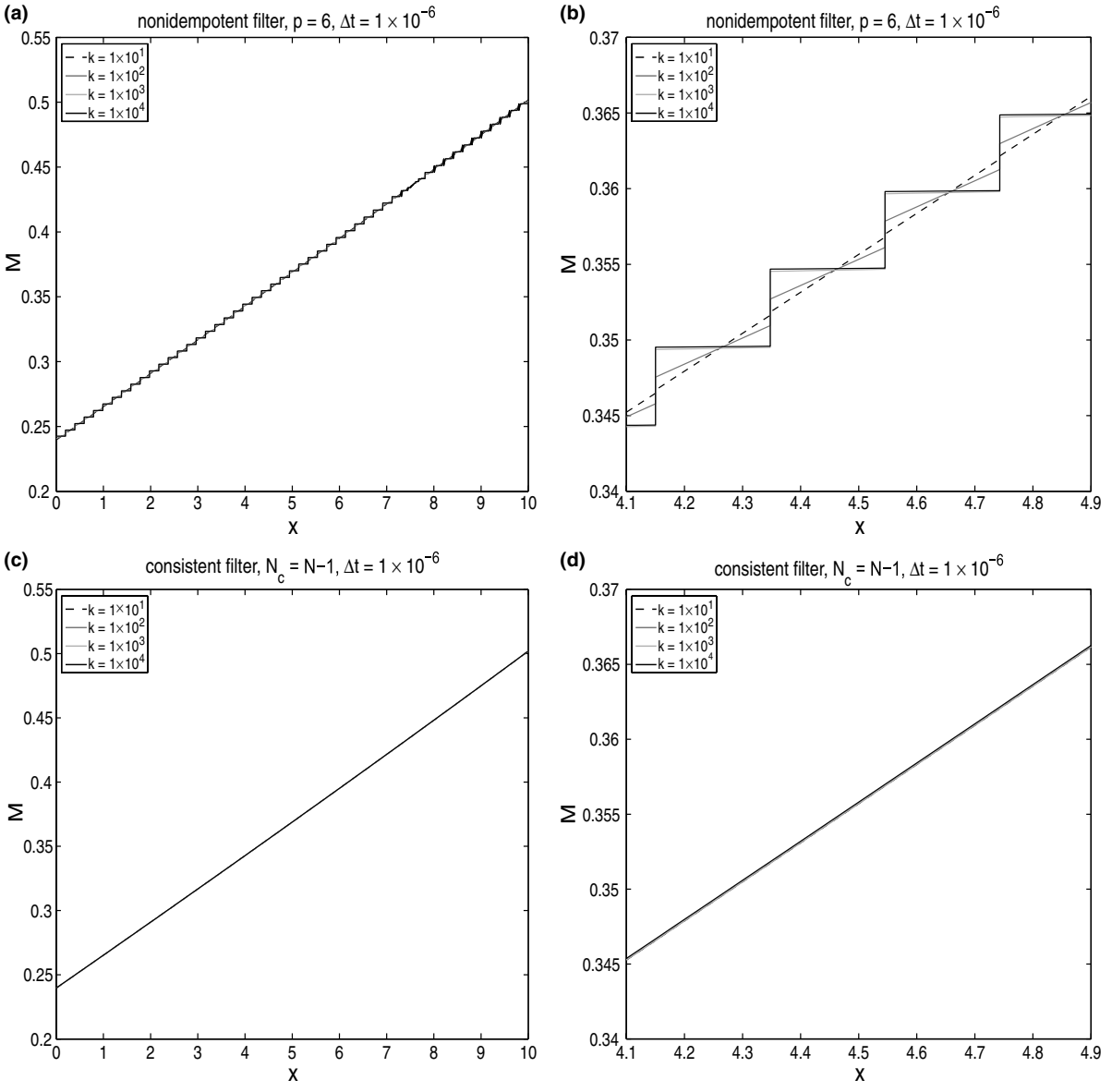

Fig. 4.3. Numerical experiments for the nonidempotent exponential filter and the idempotent sharp-cutoff filter. The top two plots show the staircase effect for nonidempotent exponential filter with filter order $p = 6$, while the bottom plots are staircase-free for the idempotent sharp-cutoff filter with $N_c = N - 1$. Polynomial degree $N = 4$ and $\Delta t = 1 \times 10^{-6}$ for all results. The plots on the right are blow-ups of the plots on the left. All figures show the Mach number profile at the centerline of the nozzle, $y = 0$.

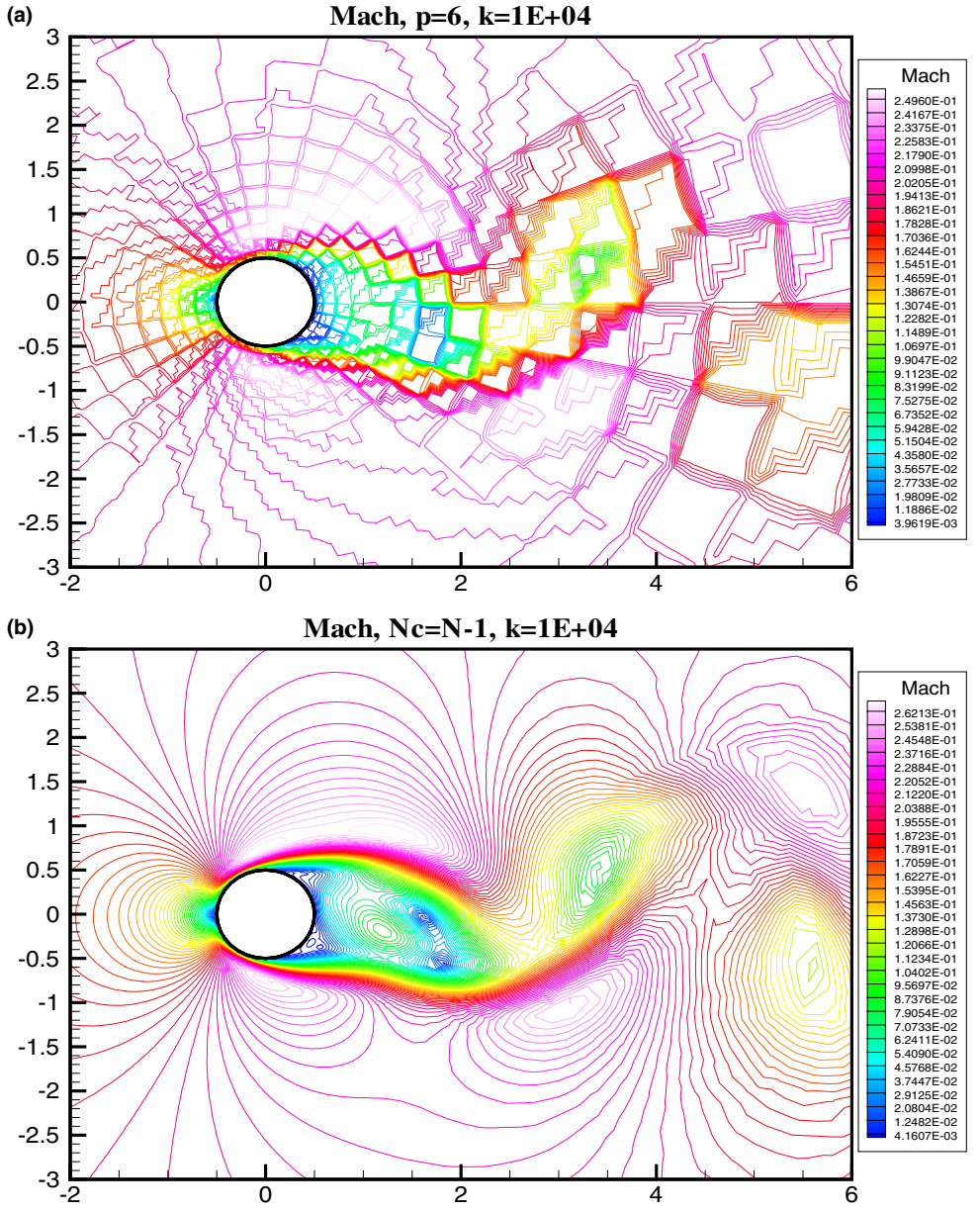

Fig. 4.4. The two plots compare the Mach contours for the cylinder vortex shedding test case at $Re = 125$. The top plot shows results for the nonidempotent exponential filter with filter order $p = 6$, while the bottom plot shows results for the sharp-cutoff filter with $N_c = N - 1$. $\Delta t = 1 \times 10^{-6}$ and polynomial degree is $N = 4$. The number of time steps $k = 10^4$.

5. Idempotent and time-consistent filters

5.1. Fundamental concepts

Definition 5.1 (*Time-consistent filter*). A time-consistent filtering process will result in the same net filter at final time $T = k_1\Delta t_1 = k_2\Delta t_2$

$$\tilde{\sigma}_{k_1\Delta t_1}(\eta) = \tilde{\sigma}_{k_2\Delta t_2}(\eta). \tag{5.21}$$

Definition 5.2 (*Idempotent filter*). An idempotent filtering process is one for which

$$\tilde{\sigma}_{k_1\Delta t}(\eta) = \tilde{\sigma}_{k_2\Delta t}(\eta) = \tilde{\sigma}_{\Delta t}(\eta). \tag{5.22}$$

If the filter is truly idempotent, it will have the same net effect after one million time steps as it does after one time step. Also, an idempotent filtering process is time-consistent. Note that if A is an idempotent operator, then $A^2 = A$.

Proposition 5.1 (Sharp-cutoff filter is idempotent). *A sharp-cutoff or step-function filter*

$$\sigma\left(\frac{n}{N}\right) = \begin{cases} 1, & 0 \leqslant n \leqslant N_c, \\ 0, & N_c < n \leqslant N. \end{cases} \tag{5.23}$$

will result in an idempotent and therefore time-consistent filtering process.

Proof. The net filter is

$$\tilde{\sigma}_{k\Delta t}\left(\frac{n}{N}\right) = \sigma^k\left(\frac{n}{N}\right) \tag{5.24}$$

$$= \begin{cases} 1^k, & 0 \leqslant n \leqslant N_c \\ 0^k, & N_c < n \leqslant N \end{cases} \tag{5.25}$$

$$= \begin{cases} 1, & 0 \leqslant n \leqslant N_c \\ 0, & N_c < n \leqslant N \end{cases} \tag{5.26}$$

$$= \sigma\left(\frac{n}{N}\right) \tag{5.27}$$

$$= \tilde{\sigma}_{\Delta t}\left(\frac{n}{N}\right). \tag{5.28}$$

The maximum possible filtering-in-time error after k steps is equal to the maximum possible filtering-in-time error after one step. □

5.2. Time-dependent filters

It is well known that the rate of convergence of the numerical approximation u_N to the analytic solution u is governed by the regularity or smoothness of the function u. If $u \in C^\infty$, then the rate of convergence is greater than any power of N (spectral convergence). However, if u is discontinuous, then the Gibbs oscillations affect the solution over the entire domain or subdomain, leading to a very slow rate of convergence. In the case of discontinuous solutions and under-resolved smooth solutions, we would still like to recover high-order accuracy in smooth regions away from the discontinuity. According to Proposition 5.1, idempotent filtering may be achieved by applying sharp-cutoff filters, but such filters have been shown to adversely affect the convergence rate of the approximation [6,21]. Vandeven [23] shows that it is possible to accelerate the rate of convergence by postprocessing u_N after each time-step iteration using a modal filter (2.5) with the following properties. Let us define a real function $\sigma(\eta) \in C^\infty[0,1]$ such that

$$\sigma(\eta): \begin{cases} \sigma(0) = 1, \\ \sigma^{(k)}(0) = 0 \quad k \leqslant p, \\ \sigma(1) = 0, \\ \sigma^{(k)}(1) = 0 \quad k \leqslant p. \end{cases} \tag{5.29}$$

Note that the properties listed in (5.29) are sufficient (not necessary) and will recover fixed-order convergence. We now consider the exponential filter function. The exponential filter does not meet all of the conditions in (5.29). However, it appears to recover high-order accuracy in practice [13]. Although we will proceed within

the framework of the exponential filter kernel, it is also possible to apply other types of filter kernels, since the precise shape of the filter does not significantly affect the accuracy [3].

It is important to point out that we are not only interested in solving steady-state problems, but in the more general case of solving time-dependent problems or problems with transient behaviour.

We propose the following: let us make our filter kernel time-dependent by allowing the order of the filter, p, to be a function of time

$$p = p(t). \tag{5.30}$$

For generality let $p_i : p_0, p_1, \ldots, p_{k-1}$ be a sequence of filter orders such that p_0 is the order of the filter applied after integrating one time step, while p_{k-1} is the order of the filter after integrating k time steps. We assume that the parameters α, N are constant for all times. The sequence of filter kernels is

$$\sigma_i\left(\frac{n}{N}\right) = \begin{cases} 1, & 0 \leqslant n \leqslant N_c, \\ \exp\left[-\alpha\left(\frac{n-N_c}{N-N_c}\right)^{p_i}\right], & N_c < n \leqslant N, \end{cases} \quad i = 0, \ldots, k-1. \tag{5.31}$$

After k time steps, our filtered approximation becomes

$$\tilde{u}_N(x, t + k\Delta t) = \sum_{n=0}^{N} (\sigma_0 \sigma_1 \sigma_2 \ldots \sigma_{k-1}) \hat{u}_n(t) \phi_n(x) \tag{5.32}$$

$$= \sum_{n=0}^{N} \left(\prod_{i=0}^{k-1} \sigma_i \right) \hat{u}_n(t) \phi_n(x) \tag{5.33}$$

$$= \begin{cases} \sum\limits_{n=0}^{N} \hat{u}_n(t) \phi_n(x), & n \leqslant N_c \\ \sum\limits_{n=0}^{N} \exp\left[-\alpha \sum\limits_{i=0}^{k-1} \left(\frac{n-N_c}{N-N_c}\right)^{p_i} \right] \hat{u}_n(t) \phi_n(x), & n \leqslant N \end{cases} \tag{5.34}$$

$$= \sum_{n=0}^{N} \tilde{\sigma}_{k\Delta t} \hat{u}_n(t) \phi_n(x). \tag{5.35}$$

Definition 5.3 (*Net filter*). In general, the net filter is defined as

$$\tilde{\sigma}_{k\Delta t}(\eta) = \prod_{i=0}^{k-1} \sigma_i(\eta). \tag{5.36}$$

The net filter is therefore

$$\tilde{\sigma}_{k\Delta t}\left(\frac{n}{N}\right) = \begin{cases} 1, & n \leqslant N_c, \\ \exp\left[-\alpha \sum\limits_{i=0}^{k-1} \left(\frac{n-N_c}{N-N_c}\right)^{p_i} \right] & n \leqslant N. \end{cases} \tag{5.37}$$

We now ask ourselves the following question: How should we choose the filter order p_i after each time step? In order for our filtering process to remain idempotent and therefore time-consistent, we must conserve the initial net filter

$$\tilde{\sigma}_{k\Delta t}(\eta) = \tilde{\sigma}_{\Delta t}(\eta). \tag{5.38}$$

Therefore, we must choose the sequence p_i such that

$$\exp\left[-\alpha \sum_{i=0}^{k-1} \left(\frac{n - N_c}{N - N_c} \right)^{p_i} \right] = \exp\left[-\alpha \left(\frac{n - N_c}{N - N_c} \right)^{p_0} \right], \quad n = N_c + 1, \ldots, N \tag{5.39}$$

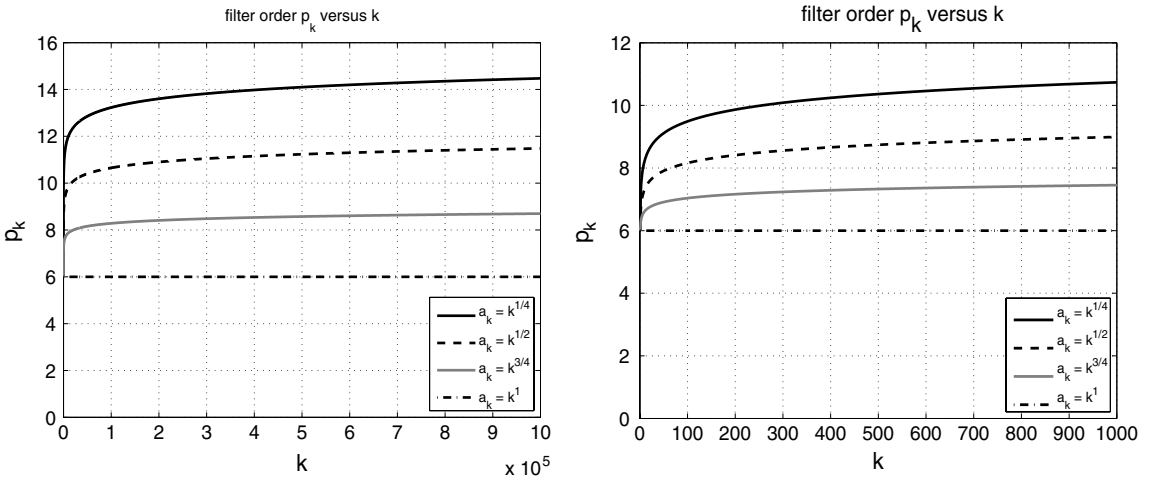

Fig. 5.5. Filter order p_k versus time step k for various choices of parameter a_k. The four curves in each plot are for $a_k = k^{1/4}, k^{1/2}, k^{3/4}, k^1$. The plot on the left is for 10^6 time steps, while the plot on the right is for 10^3 time steps. $p_0 = 6$, $\alpha = 17$, $N_c = 0$, $n_* = 1$.

or

$$\sum_{i=0}^{k-1} \left(\frac{n-N_c}{N-N_c}\right)^{p_i} = \left(\frac{n-N_c}{N-N_c}\right)^{p_0}, \quad n = N_c+1,\ldots,N. \tag{5.40}$$

However, we can see that the left-hand side is greater than the right-hand side

$$\left(\frac{n-N_c}{N-N_c}\right)^{p_0} + \sum_{i=1}^{k-1} \left(\frac{n-N_c}{N-N_c}\right)^{p_i} \geqslant \left(\frac{n-N_c}{N-N_c}\right)^{p_0}, \tag{5.41}$$

since $\frac{n-N_c}{N-N_c} \geqslant 0$. Therefore, this filtering process cannot be purely idempotent according to the definition. Nevertheless, we add coefficients a_k to the right-hand side, which can allow us to make the process less multiplicative

$$\sum_{i=0}^{k-1} \left(\frac{n-N_c}{N-N_c}\right)^{p_i} = a_k \left(\frac{n-N_c}{N-N_c}\right)^{p_0}. \tag{5.42}$$

We can rewrite this as

$$\left(\frac{n-N_c}{N-N_c}\right)^{p_{k-1}} + \sum_{i=0}^{k-2} \left(\frac{n-N_c}{N-N_c}\right)^{p_i} = a_k \left(\frac{n-N_c}{N-N_c}\right)^{p_0}. \tag{5.43}$$

Now solving for p_{k-1}

$$p_{k-1} = \frac{\log\left(a_k \left(\frac{n-N_c}{N-N_c}\right)^{p_0} - \sum_{i=0}^{k-2}\left(\frac{n-N_c}{N-N_c}\right)^{p_i}\right)}{\log\left(\frac{n-N_c}{N-N_c}\right)}, \quad k \geqslant 2,\ N_c+1 \leqslant n < N. \tag{5.44}$$

We remove the summation from the above expression for p_{k-1} by rewriting Eq. (5.44) as

$$p_{k-1} = p_0 + \frac{\log(a_k - a_{k-1})}{\log\left(\frac{n-N_c}{N-N_c}\right)}, \quad k \geqslant 2,\ N_c+1 \leqslant n < N. \tag{5.45}$$

We have an expression for p_{k-1} which depends on $n = N_c+1,\ldots,N$, N_c, p_0 and a_k. In order to retain the structure of the original filter function, which in this case happens to be the exponential filter, we cannot make p_{k-1} a function of n. In other words, we should not compute a different value of p_{k-1} for each of the $N+1$

values of n. Instead, we need to choose one value of n which will be used to compute p_{k-1}. Let us refer to this value of n as n_*.

The time-dependent exponential filter becomes

$$\sigma_{k-1}\left(\frac{n}{N}\right) = \begin{cases} 1, & 0 \leqslant n \leqslant N_c, \\ \exp\left[-\alpha\left(\frac{n-N_c}{N-N_c}\right)^{p_{k-1}}\right], & N_c < n \leqslant N, \end{cases} \tag{5.46}$$

$$p_{k-1} = p_0 + \frac{\log(a_k - a_{k-1})}{\log\left(\frac{n_*-N_c}{N-N_c}\right)}, \qquad k \geqslant 2,\ 0 \leqslant N_c < n_* < N. \tag{5.47}$$

Eq. (5.47) does not have a solution for $a_k = C$, where C is a constant. However, it does have solutions for $p_k > 0$ provided that $0 < a_k - a_{k-1} < \left(\frac{n_*-N_c}{N-N_c}\right)^{-p_0}$. We plot p_k versus k for $a_k = k^{1/4}, k^{1/2}, k^{3/4}, k^1$ in Fig. 5.5 for 10^3 and 10^6 time steps ($p_0 = 6$, $\alpha = 17$, $N_c = 0$, $n_* = 1$). We can see that $a_k = k$ results in $p_k = p_0$, which corresponds to using a constant filter order, while $a_k = k^{1/4}$ results in a filter order that ranges from $p_0 = 6$ ($k = 1$) to roughly $p = 15$ ($k = 10^6$).

Fig. 5.6 shows graphs of the filter kernel σ_k versus mode number n for $a_k = k^{3/4}$ (left) and $a_k = k^{1/4}$ (right) based on (5.46) and (5.47). The four curves in each plot are for $k = 10^0, 10^2, 10^4, 10^6$ time steps. ($p_0 = 6$, $\alpha = 17$, $N_c = 0$, $n_* = 1$). The area under the $a_k = k^{1/4}$ time-dependent filter curve grows at a significantly faster rate than that under the $a_k = k^{3/4}$ filter curve, which is expected since the corresponding filter order grows at a faster rate (Fig. 5.5).

To demonstrate that time-dependent filters can help preserve accuracy, we repeat the nozzle flow test problem using the filter based on (5.46) and (5.47) for both ERK and IMEX-RK time integration schemes. We apply the filter once per time step with the following parameters: $N_c = 0$, $n_* = 1$, $a_k = k^{3/4}$, $p_0 = 6$, $\alpha = 17$. Note that we choose $a_k = k^{3/4}$, which guarantees that $p_k \geqslant p_0$ since $0 < a_k - a_{k-1} \leqslant 1$, and results in a filter order that does not grow as quickly as $a_k = k^{1/4}$ and $a_k = k^{1/2}$ (refer to Fig. 5.5), and is more robust. We can see in Fig. 5.7 that the time-dependent exponential filter captures the shock far better than the nonidempotent filter (gray line), and produces very similar results for both the ERK (92,914 time steps) and IMEX-RK (7465 time steps) approximations.

The optimal choice of a_k, p_0, N_c and n_* for both accuracy and stability is still an open problem.

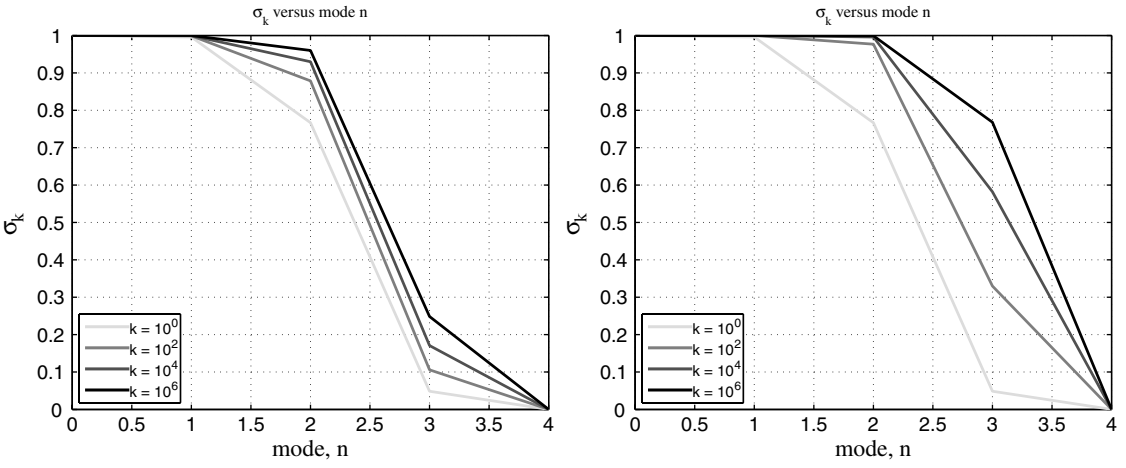

Fig. 5.6. Filter kernel σ_k versus mode number n for $a_k = k^{3/4}$ (left) and $a_k = k^{1/4}$ (right) based on (5.46) and (5.47). The four curves in each plot are for $k = 10^0, 10^2, 10^4, 10^6$ time steps. $p_0 = 6$, $\alpha = 17$, $N_c = 0$, $n_* = 1$.

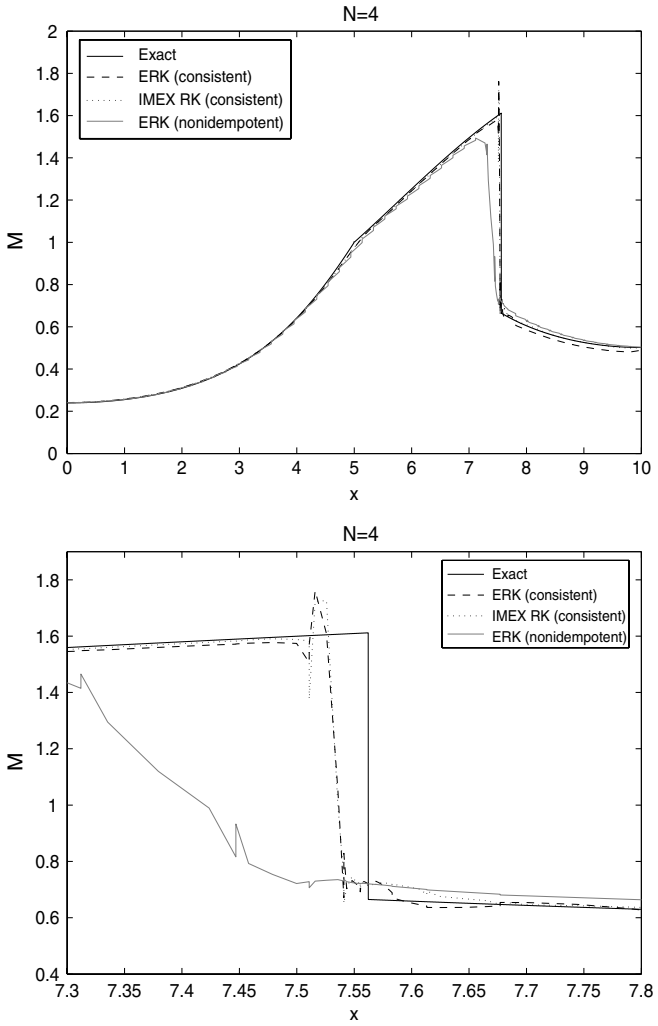

Fig. 5.7. The two figures compare the Mach number profiles at the centerline of the nozzle for the ERK and IMEX-RK numerical solutions (with time-dependent and nonidempotent exponential filters) and analytic solution. The bottom figure is a close-up of the shock region in the top figure. The polynomial degree $N = 4$ on each element. The nonidempotent exponential filter has filter order $p = 6$ and is applied once per time step. The time-dependent exponential filter is also applied once per time step and is based on (5.46) and (5.47) with the following parameters: $N_c = 0$, $n_* = 1$, $a_k = k^{3/4}$, $p_0 = 6$, $\alpha = 17$.

6. Conclusions

We identify the mechanism by which filtering can become an multiplicative process in this paper. Filtering a numerical approximation for which $\|u_N(x, t + k\Delta t) - u_N(x, t)\| \ll \| u_N(x, t)\|$ will result in a growing filtering-in-time error which will erase modes from the Fourier or polynomial approximation when nonidempotent filters are used. Purely multiplicative filtering is the worst-case scenario for time-dependent problems, and will occur if the time step is very small (e.g. due to severe stability time-step restrictions, etc.), the solution is at or near steady-state, or a combination thereof. The assumptions made in Section 3 are supported by the results in Table 4.1 for the nozzle flow example. The theory developed in Section 3 holds for time-dependent problems as long as $k\Delta t \ll t_c$, where t_c is the characteristic time-scale.

In general, filtering will erode the accuracy of the numerical approximation, but at a slower rate than that defined by the net filter (purely multiplicative) as we can see in Fig 1.1. We conjecture that the level of multiplicativity is a function of the time step Δt. The slight staircasing in Fig. 1.1 for $k = 46{,}741$ time steps looks

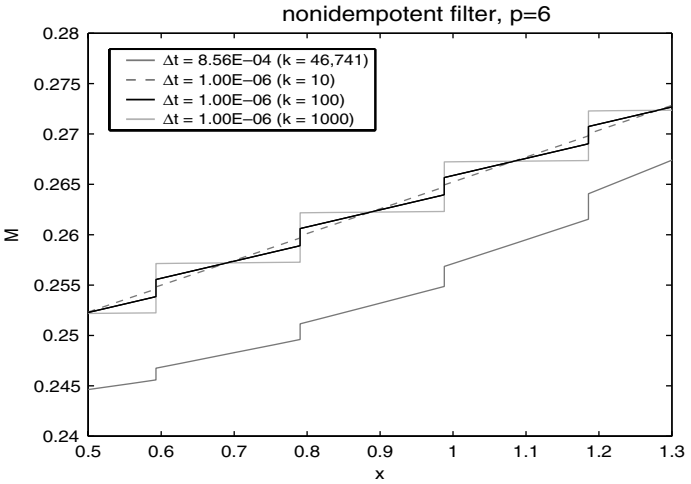

Fig. 5.8. Staircase effect for nonidempotent exponential filters with filter order $p = 6$. The single gray solid curve is the ERK solution from Fig. 1.1, while the other three curves are the test case results from Fig. 4.3.

very much like that in Fig. 4.3 for $k = 10^2$ time steps for the filter of order $p = 6$, corresponding to the net filter $\tilde{\sigma}_{100\Delta t}$. This can be seen in Fig. 5.8, where the results from Figs. 1.1 and 4.3 at the section of the nozzle where the Mach number profiles have a similar slope are plotted. The ratio of number of time steps is of the order of the ratio of the average time step sizes $\frac{46{,}741}{100} = \mathcal{O}\left(\frac{8.56\times10^{-4}}{1\times10^{-6}}\right)$. Therefore, the filtering error for the $\Delta t \approx 8.56 \times 10^{-4}$ test is roughly $\frac{8.56\times10^{-4}}{1\times10^{-6}} = 856$ times less additive than that for the $\Delta t = 1 \times 10^{-6}$ purely multiplicative test case. This means that a filtering process that is even three orders of magnitude less multiplicative than a purely multiplicative process still leads to significant loss of accuracy for long-time integration problems. A careful study needs be carried out to understand the levels of additivity of filtering errors for varying levels of $\delta = \|u_N(x, t + k\Delta t) - u_N(x, t)\|/\|u_N(x, t)\|$.

We conduct several numerical experiments in Section 4 that support the theory developed. Exponential and sharp-cutoff filters are applied for 10^4 time steps to a steady-state, inviscid compressible nozzle flow simulation governed by the two-dimensional compressible Euler equations, and a cylinder flow simulation ($Re = 125$) with periodic vortex shedding governed by the two-dimensional compressible Navier–Stokes equations. Nonidempotent exponential filters zero out all but the first couple of modes, and result in staircasing of the numerical solution, while the idempotent sharp-cutoff filter only zeros out the highest mode $n = N$. This can be seen in Figs. 4.3 and 4.4.

In Section 5, we define the concepts of time-consistent and idempotent filtering processes, and generalize the definition of the net filter for filters that may be time-dependent. A time-dependent filter (5.46) and (5.47) is constructed based on mimicking an idempotent filtering process that allows one to control the degree of the filter's multiplicity, and then tested on the nozzle flow problem. The test results, which are shown in Fig. 5.7, are nearly identical for the IMEX-RK and the ERK time integration schemes, even though the ERK test was run for roughly ten times as many time steps. Furthermore, we can see that both the ERK and IMEX-RK results with the time-dependent filter are superior at capturing the shock than the ERK results with the nonidempotent filter. It is important to mention though that determining the optimal parameters for the time-dependent filter is still an open problem and a source for future work.

To summarize, idempotent filters prevent "multiplicative" filtering . Idempotent filtering may be achieved by using sharp-cutoff filters, although sharp-cutoff filters have been shown to decrease the rate of convergence of the numerical approximation [6,21]. We suggest the development and application of time-dependent spectral filters, such as those described by (5.46) and (5.47). In the future, spatially [22] and temporally adaptive filters, for which the filter order $p = p(x, t)$ is a function of both space and time, need to be constructed for spectral and spectral element methods.

Acknowledgements

The work of A.K. was partly supported by NASA Graduate Student Researchers Program (GSRP) Fellowship NGT-1-01024 and by the NSF VIGRE Program. The work of M.H.C. was partially funded under NASA fellowship 23847923847. The work of J.S.H. was partly supported by NSF Career Award DMS-0132967 and by the Alfred P. Sloan Foundation through a Sloan Research Fellowship. The authors also thank Professor W.-S. Don, Professor D. Gottlieb, Dr. J. Grooss, Dr. S. J. Miller, Dr. R. Sendersky, and Professor C.-W. Shu for many illuminating discussions.

Appendix A

We provide some background information about the numerical test cases.

A.1. Compressible Navier–Stokes equations

We review the compressible, nondimensional Navier–Stokes equations in conservation form, which will be used to test the RK schemes described in this paper. Consider the three-dimensional Navier–Stokes equations given in Cartesian coordinates

$$\frac{\partial \mathbf{q}}{\partial t} + \nabla \cdot \mathbf{F}(\mathbf{q}) = \frac{1}{Re_{\text{ref}}}(\nabla \cdot \mathbf{F}_v), \quad t > 0. \tag{6.48}$$

The state vector $\mathbf{q}$ and the flux vector $\mathbf{F}(\mathbf{q})$ are given as

$$\mathbf{q} = \begin{bmatrix} \rho \\ \rho u \\ \rho v \\ \rho w \\ E \end{bmatrix}, \quad \mathbf{F}(\mathbf{q}) = \begin{bmatrix} \rho u \\ \rho u^2 + p \\ \rho uv \\ \rho uw \\ (E+p)u \end{bmatrix} \hat{i} + \begin{bmatrix} \rho v \\ \rho uv \\ \rho v^2 + p \\ \rho vw \\ (E+p)v \end{bmatrix} \hat{j} + \begin{bmatrix} \rho w \\ \rho uw \\ \rho vw \\ \rho w^2 + p \\ (E+p)w \end{bmatrix} \hat{k}, \tag{6.49}$$

where ρ is density, u, v and w are the Cartesian velocity components, E is the total energy, and p is the pressure. The total energy

$$E = \rho\left(T + \frac{1}{2}(u^2 + v^2 + w^2)\right). \tag{6.50}$$

The pressure and temperature are related through the ideal gas law

$$p = (\gamma - 1)\rho T, \tag{6.51}$$

where T is the temperature and $\gamma = c_p/c_v$ is the ratio between the constant pressure (c_p) and constant volume (c_v) heat capacities. $\gamma = 1.4$ for air. The viscous vector is

$$\mathbf{F}_v = \begin{bmatrix} 0 \\ \tau_{xx} \\ \tau_{yx} \\ \tau_{zx} \\ \tau_{xx}u + \tau_{yx}v + \tau_{zx}w + \frac{\gamma k}{Pr}\frac{\partial T}{\partial x} \end{bmatrix} \hat{i} + \begin{bmatrix} 0 \\ \tau_{xy} \\ \tau_{yy} \\ \tau_{zy} \\ \tau_{xy}u + \tau_{yy}v + \tau_{zy}w + \frac{\gamma k}{Pr}\frac{\partial T}{\partial y} \end{bmatrix} \hat{j} \tag{6.52}$$

$$+ \begin{bmatrix} 0 \\ \tau_{xz} \\ \tau_{yz} \\ \tau_{zz} \\ \tau_{xz}u + \tau_{yz}v + \tau_{zz}w + \frac{\gamma k}{Pr}\frac{\partial T}{\partial z} \end{bmatrix} \hat{k}. \tag{6.53}$$

We assume that the fluid is Newtonian, for which the stress tensor is defined as

$$\tau_{x_i x_j} = \mu\left(\frac{\partial u_i}{\partial x_j} + \frac{\partial u_j}{\partial x_i}\right) + \delta_{ij}\lambda\sum_{k=1}^{3}\frac{\partial u_k}{\partial x_k}, \tag{6.54}$$

where μ is the dynamic viscosity, λ is the coefficient of Bulk viscosity for the fluid, and k is the coefficient of thermal conductivity. We use Sutherland's law to relate the dynamic viscosity to the temperature

$$\frac{\mu(T)}{\mu_s} = \left(\frac{T}{T_s}\right)^{\frac{3}{2}}\frac{T_s + S}{T + S}, \tag{6.55}$$

where $\mu_s = 1.716 \times 10^{-5}$ kg/m s, $T_s = 273$ K, $S = 111$ K and the Prandtl number $Pr = .72$ for atmospheric air. Stokes hypothesis gives us $\lambda = -\frac{2}{3}\mu$.

We normalize Eq. (6.50) using reference values $u_{\text{ref}} = u_0$, $\rho_{\text{ref}} = \rho_0$, $p_{\text{ref}} = \rho_0 u_0^2$, $T_{\text{ref}} = u_0^2/c_v$ and L as the reference length. Therefore, the reference Reynolds number $Re_{\text{ref}} = \frac{\rho_0 u_0 L}{\mu_0}$ and the Prandtl number $Pr = \frac{c_p \mu_0}{k_0}$.

A.2. Two-dimensional nozzle flows

Consider the two-dimensional Euler equations given in conservation form

$$\frac{\partial \mathbf{q}}{\partial t} + \nabla \cdot \mathbf{F}(\mathbf{q}) = 0. \tag{6.56}$$

The state vector $\mathbf{q}$ and the flux vector $\mathbf{F}(\mathbf{q})$ are given in Section A.1 for the three-dimensional Euler equations. For the two-dimensional Euler equations, the state vector is

$$\mathbf{q} = [\rho, \rho u, \rho v, E]. \tag{6.57}$$

We consider the flow in a two-dimensional duct (rectangular cross-section) or nozzle, modeled using the Euler equations. We solve the two-dimensional compressible Euler equations using both ERK and IMEX-RK time-stepping schemes and compare the accuracy and efficiency of both schemes. The converging-diverging nozzle (Fig. 1.1) has an area $A(x)$ given by

$$A(x) = \begin{cases} 1.75 - .75\cos((.2x - 1.0)\pi), & 0 \leqslant x \leqslant 5, \\ 1.25 - .25\cos((.2x - 1.0)\pi), & 5 \leqslant x \leqslant 10. \end{cases} \tag{6.58}$$

This is a classic one-dimensional steady (steady-state), inviscid compressible flow problem that has an analytic solution [1] on the centerline at $y = 0$. The initial condition is a linear profile that connects the exact (analytic) boundary conditions at $x = 0$ and $x = 10$.

A ratio between the stagnation pressure and the back pressure of .75 (back pressure/stagnation pressure) results in a choked flow with a stationary normal shock in the divergent part of the nozzle at $x \cong 7.56$. The Mach number $M = 1.0$ and the stagnation temperature $T = 300$ K as the flow is choked. The inflow Mach number $M = .240$ and the outflow Mach number $M = .501$.

A.3. Navier Stokes equations: cylinder flow

Consider the two-dimensional Navier–Stokes equations given in conservation form

$$\frac{\partial \mathbf{q}}{\partial t} + \nabla \cdot \mathbf{F}(\mathbf{q}) = \frac{1}{Re_{\text{ref}}}(\nabla \cdot \mathbf{F}_v). \tag{6.59}$$

The state vector $\mathbf{q}$ and the flux vector $\mathbf{F}(\mathbf{q})$ are given in Section A.1 for the three-dimensional Navier–Stokes equations. For the two-dimensional Navier–Stokes equations, the state vector is

$$\mathbf{q} = [\rho, \rho u, \rho v, E]. \tag{6.60}$$

Two-dimensional flow around a cylinder predicted by the 2D NS equations has good agreement with experimental results up to Reynolds numbers of roughly $Re = 180$. For $Re > 180$, three-dimensional effects take place, and numerical results can no longer be validated against experimental results. We perform calculations at $Re = 125$. We run the test with polynomials of degree $N = 4$ until time $T = 150$, by which periodic vortex shedding is well established. The computational domain is a disk with radius equal to approximately 20 cylinder diameters.

A.4. Numerical scheme

We follow the method of lines approach, and discretize the spatial operators using a nodal discontinuous Galerkin method based on [7,14,15].

The local approximation in each subdomain D is the Nth-degree polynomial

$$p_N(x) = \sum_{k=1}^{(N+1)(N+2)/2} p_N(x_k) L_k(x), \tag{6.61}$$

where x_k are the $(N+1)(N+2)/2$ Hesthaven electrostatic points [12] in each domain, $L_k(x)$, $k \in [1, \ldots, (N+1)(N+2)/2]$ is the local polynomial basis, and the subdomains D are linear triangular elements. The flux is approximated as

$$F_N(p_N) = \sum_{k=1}^{(N+1)(N+2)/2} F_N(p_N(x_k)) L_k(x). \tag{6.62}$$

We require that the equation be satisfied on each element in the following discontinuous Galerkin way

$$\int_D \left(\frac{\partial p_N}{\partial t} + \nabla \cdot F_N \right) L_k(x)\,\mathrm{d}x = \oint_{\delta D} L_k(x) \hat{n} \cdot [F_N - F_N^*]\,\mathrm{d}x. \tag{6.63}$$

We use a local Lax-Friedrichs numerical flux

$$F_N^* = \frac{F_N(p_N^+) + F_N(p_N^-)}{2} - \frac{|\lambda|}{2}(p_N^+ - p_N^-), \tag{6.64}$$

where $|\lambda|$ is the maximum local eigenvalue of the flux Jacobian

$$|\lambda| = \max_{p_N^+, p_N^-}(|\mathbf{u}| + c) = \max_{p_N^+, p_N^-} \left(\sqrt{u^2 + v^2} + \sqrt{|\gamma p/\rho|} \right). \tag{6.65}$$

p_N^+ is the local solution, while p_N^- is the solution in the neighboring element.

To integrate the resulting system of ODEs in time, we use a 4th-order low-storage explicit Runge–Kutta method [5] for all numerical experiments in this paper. For IMEX-RK results, we use the 4th-order Additive Runge–Kutta scheme, ARK4(3) [18].

Note that for the nozzle flow test case, the filter is applied once per time step (at the end of time step), while for the cylinder flow test case the filter is applied once per Runge–Kutta stage (at the end of each stage).

References

[1] J.D. Anderson, Modern Compressible Flow, McGraw-Hill, New York, 2002.
[2] J.P. Boyd, Chebyshev and Fourier Spectral Methods, second ed., Dover, New York, 2001.
[3] J.P. Boyd, The Erfc-Log filter and the asymptotics of the Euler and Vandeven sequence accelerations, in: A.V. Ilin, L.R. Scott (Eds.), Proceedings of the Third International Conference on Spectral and High Order Methods, Houston J. Mathematics, Houston, 1996, pp. 267–276.
[4] C. Canuto, M.Y. Hussaini, A. Quarteroni, T.A. Zang, Spectral Methods in Fluid DynamicsSpringer Series in Computational Physics, Springer, New York, 1988.
[5] M.H. Carpenter, C.A. Kennedy, Fourth-Order 2*N*-Storage Runge–Kutta Schemes, NASA-TM-109112, 1994, pp. 1–24.
[6] P.F. Fischer, J.S. Mullen, Filter-based stabilization of spectral element methods, C. R. Acad. Sci. Sér. I - Anal. Numér. 332 (2001) 265–270.

[7] F.X. Giraldo, J.S. Hesthaven, T. Warburton, Nodal high-order discontinuous Galerkin methods for the spherical shallow water equations, J. Comput. Phys. 181 (2002) 499–525.
[8] D. Gottlieb, J.S. Hesthaven, Spectral methods for hyperbolic problems, J. Comput. Appl. Math. 128 (2001) 83–131.
[9] D. Gottlieb, S. Orszag, Numerical analysis of spectral methods: theory and applications, SIAM Monograph, 1977.
[10] D. Gottlieb, C.-W. Shu, On the Gibbs phenomenon and its resolution, SIAM Rev. 39 (1997) 644–668.
[11] D. Gottlieb, C.-W. Shu, A. Solomonoff, H. Vandeven, On the Gibbs phenomenon I. Recovering exponential accuracy from the Fourier partial sum of a nonperiodic analytic function, J. Comput. Appl. Math. 43 (1992) 81–98.
[12] J.S. Hesthaven, From electrostatics to almost optimal nodal sets for polynomial interpolation in a simplex, SIAM J. Numer. Anal. 35 (2) (1998) 655–676.
[13] J.S. Hesthaven, R.M. Kirby, Filtering in Legendre spectral methods, Math. Comput. (submitted).
[14] J.S. Hesthaven, T. Warburton, Nodal high-order methods on unstructured grids I: Time-domain solution of Maxwell's equations, J. Comput. Phys. 181 (2002) 186–221.
[15] J.S. Hesthaven, T. Warburton, Discontinuous Galerkin methods for the time-domain Maxwell's equations: an introduction, ACES Newsletter 19 (2004) 12–30.
[16] A. Kanevsky, High-order implicit–explicit Runge–Kutta time integration schemes and time-consistent filtering in spectral methods, Brown University PhD Thesis, 2006, pp. 1–138.
[17] A. Kanevsky, M.H. Carpenter, D. Gottlieb, J.S. Hesthaven, High-order implicit–explicit Runge–Kutta discontinuous Galerkin methods for fluid flows (in preparation).
[18] C.A. Kennedy, M.H. Carpenter, Additive Runge–Kutta schemes for convection–diffusion–reaction equations, Appl. Numer. Math. 44 (2003) 139–181.
[19] H.O. Kreiss, J. Oliger, Stability of the Fourier method, SIAM J. Numer. Anal. 16 (1979) 421–433.
[20] A. Majda, J. McDonough, S. Osher, The Fourier method for nonsmooth initial data, Math. Comput. 32 (1978) 1041–1081.
[21] C.-W. Shu, W.-S. Don, D. Gottlieb, O. Schilling, L. Jameson, Numerical convergence study of nearly incompressible, inviscid Taylor-Green vortex flow, J. Sci. Comput. 24 (2005) 1–27.
[22] E. Tadmor, J. Tanner, Adaptive mollifiers – high resolution recovery of piecewise smooth data from its spectral information, Foundat. Comput. Math. 2 (2002) 155–189.
[23] H. Vandeven, Family of spectral filters for discontinuous problems, J. Sci. Comput. 6 (1991) 159–192.